Observation of Excitonic Super-radiance in Quantum Well Structures and its Application for Laser Cooling of Solids

Iman Hassani nia[1], David Weinberg[2], Skylar Wheaton[1], Emily A. Weiss[2] and Hooman Mohseni[1]

[1]*Bio-Inspired Sensors and Optoelectronics Laboratory, EECS Department, Northwestern University, Evanston, Illinois, USA*

[2]*Department of Chemistry, Northwestern University, Evanston, Illinois, USA*

[a)]*Email: hmohseni@ece.northwestern.edu Tel:847-491-7727 , Fax:847-491-4455*

keywords: Quantum wells, Excitonic super-radiance, Excitons, Carrier density, Radiative lifetime

Abstract:

Excitons, bound electron-hole pairs, possess distinct physical properties from free electrons and holes that can be employed to improve the performance of optoelectronic devices. In particular, the signatures of excitons are enhanced optical absorption and radiative emission. These characteristics could be of major benefit for the laser cooling of semiconductors, a process which has stringent requirements on the parasitic absorption of incident radiation and the internal quantum efficiency. Here we experimentally demonstrate the dominant ultrafast excitonic super-radiance of our quantum well structure from 78 K up to room temperature. The experimental results are followed by our detailed discussions about the advantages and limitations of this method.

1-Introduction

Optical refrigeration of solids is emerging as a viable solution for future cooling purposes especially for satellite and airborne applications[1]. The key advantage of this method is the lack of the vibration and its compactness when compared to mechanical refrigerators or cryo-coolers that utilize cryogenic liquids[2]. These characteristics have motivated researchers to realize practical semiconductor laser refrigerators during the last two decades following the first observation of optical refrigeration in ytterbium doped glass in 1995[3]. However due to the insufficient material quality this effect was not realized until recently in CdS nanobelts that exhibited an internal quantum efficiency very close to 100%[4]. To give insight on the necessity for such an ultra-high material quality we note that the cooling efficiency (η_c) is equal to[5]:

$$\eta_c = \eta_{ext}(1 + kT / E_g) - 1 \qquad (1)$$

where k is the Boltzmann constant, T is the temperature , E_g is the bandgap and η_{ext} is the external quantum efficiency which is equal to[5]:

$$\eta_{ext} = \frac{\eta_e B n^2}{\eta_e B n^2 + An + Cn^3} \qquad (2)$$

Where η_e is the extraction efficiency, B is the radiative, A is the Shockley-Reed-Hall and C is the Auger recombination coefficient of the material. Since kT/E_g is usually very low (equal to almost 1.7×10^{-3} for GaAs at room temperature), therefore it can be inferred from Eq (1) and (2) that in order to achieve laser cooling, the external quantum efficiency should be very close to 100%. This imposes a though condition on material quality and in particular necessitates a very low Shockley-Reed-Hall recombination. It should be noted that Eq (2) pertains to the case of plasma radiative process. In this paper we focus on the radiative recombination of excitons known as

Optical and Electronic Cooling of Solids, edited by Richard I. Epstein, Denis V. Seletskiy, Mansoor Sheik-Bahae, Proc. of SPIE Vol. 9765, 97650J · © 2016 SPIE
CCC code: 0277-786X/16/$18 · doi: 10.1117/12.2211982

excitonic supper radiance [6] which as shown by Ref[7], is significantly larger than the free plasma counterpart. This paper is organized as follows. In section 2, we re-introduce the excitonic supper radiance mechanism and the effect of exciton thermalization. Next, to make it suitable for laser cooling, we point to polaritonic crystals as a way to extract the energy of exciton-polaritons through radiation to free space. Our proposal is backed by finite difference time domain (FDTD) simulations which are used to find the bandstructure and the extraction efficiency enhancement. In section 3, we present our measurement results and our analysis and interoperations. The signature of excitonic supper radiance is detected and the potential of laser cooling in such material system is explored. Finally we conclude the paper in section 4.

2-Excitonic super-radiance and its applications for laser cooling of solid

Excitons are bound electron and hole pairs just like hydrogen atoms whereas the free electron hole plasma can be compared to ionized hydrogen atoms. Due to the fact that electron and holes are closer to each other in the form of an exciton, the optical oscillator strength of excitons in significantly larger in these species compared to the free plasma. This results in the well-known enhanced excitonic absorption and, as we shall see, to an enhanced radiation. Andreani et al[7] used the Einstein relation to find the spontaneous radiative rate (R_{sp}) of excitons:

$$R_{sp} = \left(\frac{2\pi}{\hbar}\right)|H_{21}|^2 N(E_{21}) f_2(1-f_1) \tag{3}$$

Where $\hbar$ is the reduced Planck's constant, H_{21} is the interaction dipole matrix element of the Hamiltonian of the whole system comprising the photons and the material. $N(E_{21})$ is the photonic density of states for the emitted photons that have energy equal to the transition energy (E_{21}) and lastly f_2 and f_1 denote the occupation probability of the excited and the ground electronic states respectively. In the following derivations, we assume that f_2=1 and f_1=0.

We note that in a bulk material the excitons cannot release energy in the form of free photons to the far field[7]. Rather they bind with photons to form exciton-polaritons. This is a consequence of conservation of momentum. However in quantum wells, the crystal symmetry is broken along the direction of the epitaxial growth. Therefore the conservation of momentum does not hold in this direction which allows the "heavy" excitons to be converted to free "light" photons. This has been referred to as the so called excitonic super-radiance in QWs[6]. To derive the formula for excitonic superradiance in QW structure, the photonic density of states introduced in Eq (3) should satisfy the following conditions: 1- the energy of the photons is equal to the exciton resonance energy which determines the wavevector (k_0) of the photons radiated into free space 2- due to conservation of the in-plane wavevector ($k_{||}$) of the excitonic radiative decay, in order to have a propagative optical power transfer to the free space, the in-plane wavevector should be smaller than the total wavevector (k_0). By counting the states (per unit energy and volume) that satisfy the aforementioned conditions one can obtain[7]:

$$\Gamma_T = \frac{\pi}{n_r}\frac{q^2}{m_0 c} f_{xy}\left(\frac{k_0}{\sqrt{k_0^2 - k_{\|}^2}}\right) \tag{4}$$

where, n_r is the refractive index, q is the electron charge, m_0 is the free mass of the electron, c is the speed of light and f_{xy} is the dipole oscillator strength per unit area. The above equation is valid for transverse exciton polaritons whose polarization is in the plane of the quantum well and is orthogonal to the direction of their $k_{||}$. in order to obtain the radiative rate of the longitudinal polaritons (with polarization parallel to $k_{||}$), a projection factor has to be multiplied to right hand side of Eq(4) , to take into account only the component that has the polarization orthogonal to the resulting photon propagation direction (the direction of k_0) . Therefore we obtain:

$$\Gamma_L = \frac{\pi}{n}\frac{q^2}{m_0 c} f_{xy}\left(\frac{\sqrt{k_0^2 - k_{\|}^2}}{k_0}\right) \tag{5}$$

And similarly when the polarization of the exciton is along the direction of growth, we have:

$$\Gamma_z = \frac{\pi}{n}\frac{q^2}{m_0 c} f_z\left(\frac{k_\parallel^2}{k_0\sqrt{k_0^2-k_\parallel^2}}\right) \tag{6}$$

Here the oscillator strength denoted by f_z is different from f_{xy} because only light-hole excitons can emit in this case and they possess weaker oscillator strength. In our QW structure the optical transition is caused by heavy-hole excitons and for the case of $k_{||}$=0, we obtain the superradiance rate of 4×10^{10} s^{-1} which is more than four orders of magnitude larger than the Shockley-read-hall , granting an external quantum efficiency of almost 100%! However for achieving optical refrigeration, blueshift of the radiation is also required[8]. To investigate this, we first note that similar to free plasma, excitons can also gain energy from phonons and thermalize, as a result they can possess higher energy and larger wavevectors. If we compare the maximum kinetic energy of the excitons which can radiate (equal to $\frac{\hbar^2 k_0^2}{2M}$ where M is the mass of the exciton) to the average kinetic energy of the excitons at equilibrium (approximately equal to kT), we notice that the latter is significantly larger. This means that only a small fraction of excitons can decay radiatively. This small fraction decreases linearly with the increase in temperature as the characteristic energy kT grows. A weighted average over the radiative rate of the all of the heavy-hole excitons gives:

$$\Gamma(T) = \frac{\hbar^2 k_0^2}{3MkT}\Gamma_0 \tag{7}$$

In which Γ_0 is the equal to Γ_L or Γ_T for normal radiation ($k_{||}$=0). After considering the effect of thermalization we figure out that the radiative rate of the excitons drops by two orders of magnetude. On the other hand the large superraince decay rate of excitons with $k_\parallel < k_0$ (equal to 4×10^{10} s^{-1}) is almost futile since for these excitons the maximum excess energy obtained by absorbing phonons is equal to $\frac{\hbar^2 k_0^2}{2M} \approx 1.1\,K$ which is a negligible value! Therefore creative methods are required to convert the energy of the exciton-polaritons to radiative photons. Here we introduce the concept of polaritonic crystal to achieve this aim. In such a structure the guided modes can undergo Bragg reflections as shown schematically in Fig. These Bragg reflections can make the polariton mode radiative only if:

$$\left|K_{\parallel m} + pG\right| < k_0 \tag{8}$$

Where $K_{\parallel m}$ is the in-plane wavevector of the m^{th} guided mode of the membrane, p is the order of refraction and G is the reciprocal lattice wavevector. The reciprocal lattice shown in Fig.1 demonstrates this idea. If the polariton undergoes a Bragg reflection such that the above condition is satisfied, it will be diffracted to air effectively. To determine the coupling efficiency to the polaritonic crystal, we have performed FDTD simulations to determine the

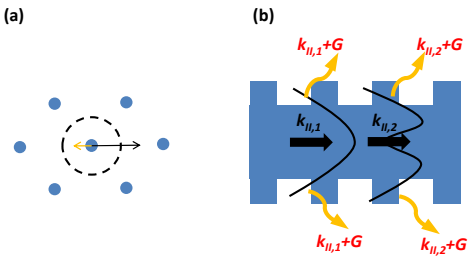

Fig.1 (a) reciprocal lattice, a Bragg reflection can make the wavevector above the light line (the area enclosed by the dashed circle). (b) Schematics of Bragg reflections in a polaritonic crystal slab.

bandstructure and the extraction efficiency. We have used the effective permittivity of the heavy-hole excitons for the QW structure for these simulations[9]. Consider a membrane with the QW structure in the middle that has a width of 100 nm and a hexagonal array of holes forming the polaritonic crystal as shown in Figure 2(a). The period of the polaritonic crystal is 500 nm and the radius of the holes is equal to 130 nm and their depth is 50 nm, they are etched up to the QW and are on both sides of the membrane. Figure 2(b), (c) shows the bandstructure with and without the excitonic resonance (when the refractive index of the QW is set to 3.4). One can notice a strong resonance as indicated by the horizontal line around the excitonic resonance frequency which is also observed in bandstructure calculations of Ref[10] . This allows a wide range of in-plane polaritonic wavevectors near the resonance. The area above the light cone is diffracted into the air. It can be seen that the presence of the polaritonic crystal results in bands that not only span the energy of the thermalized polaritons but also they are above the light cone. To determine the extraction efficiency, we have simulated a membrane with and without the polaritonic crystal by placing a point source with in-plane polarization (characteristic of heavy hole excitons) in the middle of structure. Perfectly matched layer (PML) boundary condition were applied to all boundaries. The power monitors on the top and the bottom of the membrane were used to obtain the extracted power. This simulation results suggested an enhancement of 3.5. We roughly approximate this increase in the average radiative decay to the extraction of the excitons which have 3.5 times higher kinetic energy. These excitons could not decay radiatively without the presence of the photonic crystal. As a result in this case the excess energy is …. times higher. This significant improvement was achieved even without optimizing the polaritonic crystal that can be the subject of future research.

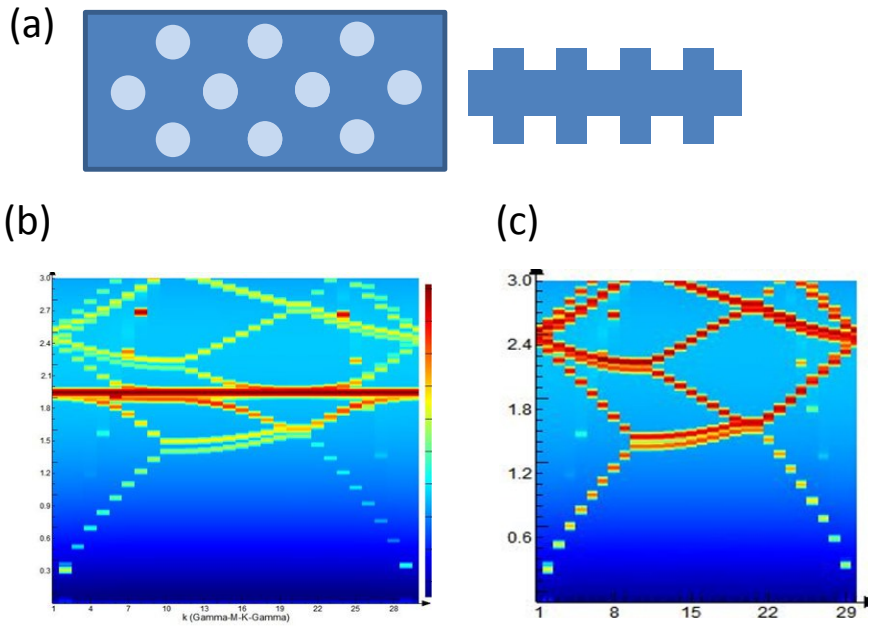

Figure 2 (a) The geometry of the simulated polaritonic crystal (b) the simulated bandstructure of the polaritonic crystal with the excitonic refractive index (c) same simulation as in (b) but the refractive index of the active region is assumed to be constant.

3- Experimental setup and measurements

We have performed intensity-dependent and time-resolved PL measurements for two samples. These samples contain MQW structures as listed in Table. I and Table. II. Metal organic chemical vapor deposition (MOCVD) was used to grow the MQW structures. We have performed time-correlated photon counting techniques (TCSPC) to obtain the time resolved PL spectra at low excitation powers as shown in Figure 3. One can notice a big difference

Table I. the layer structure of sample VE1946c.

Layer #		Material	Thickness (nm)	Doping	Comment
1		InP		n-doped	Substrate
2		$In_{0.53}Ga_{0.47}As$	100	$N=10^{18}$ cm^{-3}	Absorber
3		InP	1000	Ramped $N=10^{18}$ cm^{-3} to $N=10^{17}$	Bottom Cladd
4		InP	500	$N=10^{17}$ cm^{-3}	Transition
5X	*1*	$In_{0.53}Al_{0.47}As$	17	undoped	Quantum well first layer
	2	Q 1.43	18	undoped	Quantum well second layer
	3	$In_{0.53}Al_{0.47}As$	1	undoped	Quantum well third layer
	4	$In_{0.53}Ga_{0.47}As$	3	undoped	Quantum well fourth layer
	5	InP	17	undoped	Quantum well fifth layer
6		InP	500	$P=10^{17}$ cm^{-3}	Top cladd layer
7		Q 1.2	15	$P=10^{17}cm^{-3}$	Etch stop layer
8		InP	1000	$P=10^{17}$ cm^{-3} Ramped up to $P=10^{18}$	Top cladd layer
9		$In_{0.53}Ga_{0.47}As$	50	$P=2x10^{18}cm^{-3}$	Top contact

Table.II the layer structure of sample VE2956c

Layer #		Material	Thickness (nm)	Doping	Comment
1		InP		Semi-insulating	Semi-insulating Substrate
	2	Lattice-matched InGaAs	10	Un-doped	Quantum well second layer
	3	InP	20	Un-doped	Quantum well third layer
2		InP	500	Un-doped	Top cladd layer

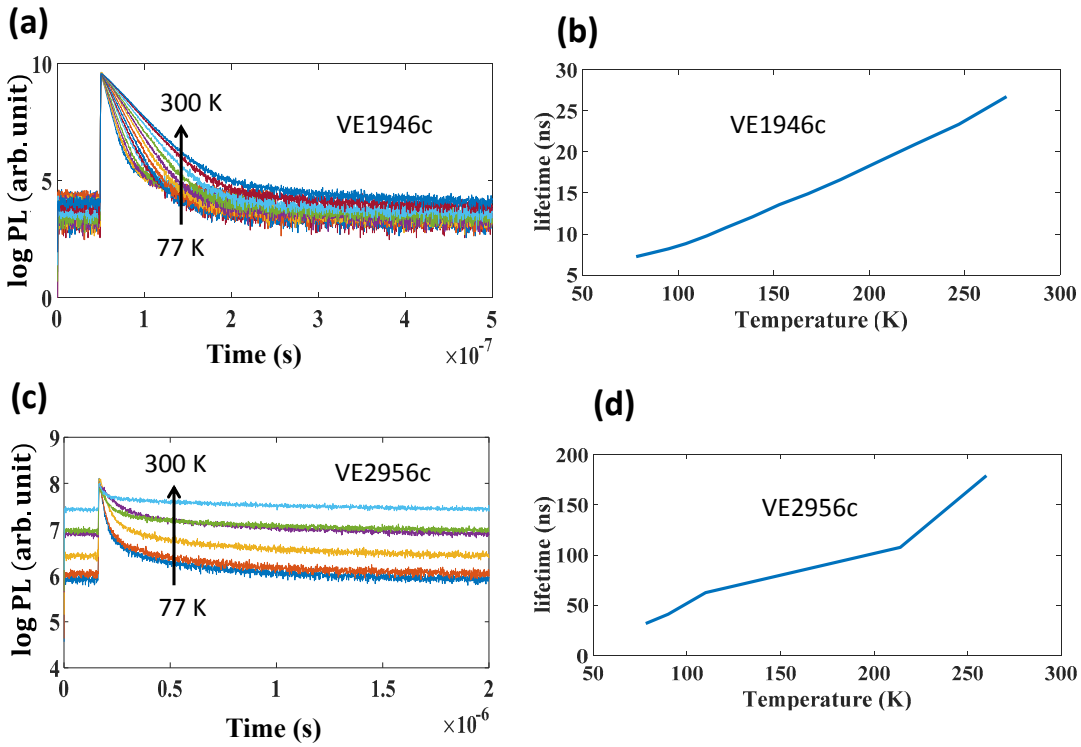

Figure 3 Logarithmic amplitude of PL versus time for sample VE1946c as obtained by TCSPC measurements (b) the PL lifetimes versus temperature calculated based on the measurements in (a), (c) Logarithmic amplitude of PL versus time for sample VE2956c as obtained by the TCSPC (d) the PL lifetimes versus temperature calculated based on the measurements in (c).

for the behavior of the lifetime versus temperature of both samples. While for the sample VE2956c (lattice-matched InGaAs/InP quantum well structure) the lifetime follows the relation $T^{-1.5}$ with temperature which is a characteristic of the radiative recombination rate of free plasma , for the sample VE1946c a linear dependence with the temperature was observed which is a characteristic of excitonic superradiance as shown by Eq(6) . For both samples the luminescence increased by decreasing the temperature. To have a better understanding of the underlying phenomena, we performed intensity dependent experiments using a calibrated integrating sphere as shown schematically in Figure 4. This setup can be used to estimate the external quantum efficiency of the samples by measuring the total photoluminescence (PL) power coming out of the sample. To measure the absorption we used Agilent carry 5000 spectrophotometer.

It should be noted that the internal quantum efficiency of the samples can be determined once the extraction efficiency is known. We have found the extraction efficiency based on the measured absorbance of the sample and the ray tracing performed by ZEMAX, the results are tabulated in Table III. The results for the un-processed planar sample are comparable with the rough estimation of $1/2n^2$. The results after attaching the hemisphere lens with various materials and refractive indices are also shown. We note that in general the extraction efficiency is also a function of internal quantum efficiency because of the photon reabsorption and remission. The calculated extraction efficiency for the planar wafers were used to estimate the internal quantum efficiency as shown in Figure 5 . Again we see a big difference for the internal quantum efficiency of both samples versus the excitation power. For sample VE2956c the curve shows a linear response whereas for sample VE1946c its variation over the excitation power range is not significant. For the 980 nm excitation laser, we performed a transmission measurement using the same

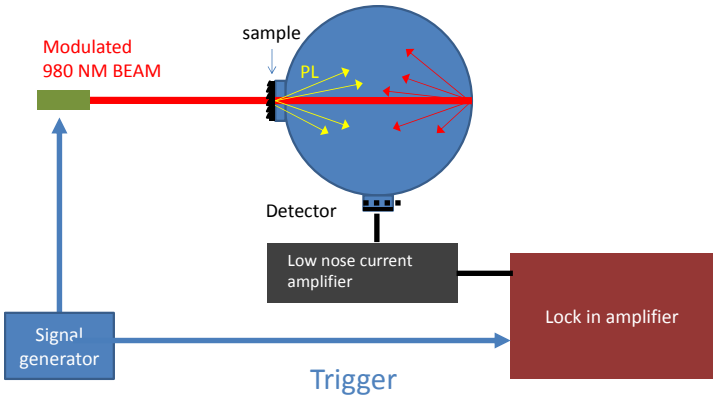

Figure 4 Schematics of the setup for intensity-dependent PL measurements

setup for both samples and it turned out that the absorption of both samples doesn't change within this range and therefore cannot be responsible for the observed behavior. We have compared the results with those suggested by analytical evaluation of Ref [11] and we identified the possible region of operation for both samples. Furthermore we implemented the method of curve fitting to obtain the recombination parameters as described by Ref[11]. In this method the radiative recombination rate is found analytically whereas the Shockley-Reed hall recombination coefficient is found by curve fitting. For sample VE2956c, we obtained the recombination parameters shown in

Table.III The extraction efficiency foe sample with different hemisphere lenses

sample #	**Hemisphere lens**	**coating**	**Extraction efficiency**
VE1946c	No lens	No coating	3.2%
VE1946c	InP hemisphere lens, refractive index=3.4 , diameter 1 cm	No coating	83%
VE1946c	InP hemisphere lens, refractive index=3.4 , diameter 1 cm	$\lambda/4$ AR coating	86%
VE1946c	ZnSe hemisphere lens, refractive index=2.5 , diameter 1 cm	No coating	28%
VE2956c	No lens	No coating	3.85%
VE2956c	InP hemisphere lens, refractive index=3.4 , diameter 1 cm	No coating	92%
VE2956c	InP hemisphere lens, refractive index=3.4 , diameter 1 cm	$\lambda/4$ AR coating	96%
VE2956c	ZnSe hemisphere lens, refractive index=2.5 , diameter 1 cm	No coating	28%

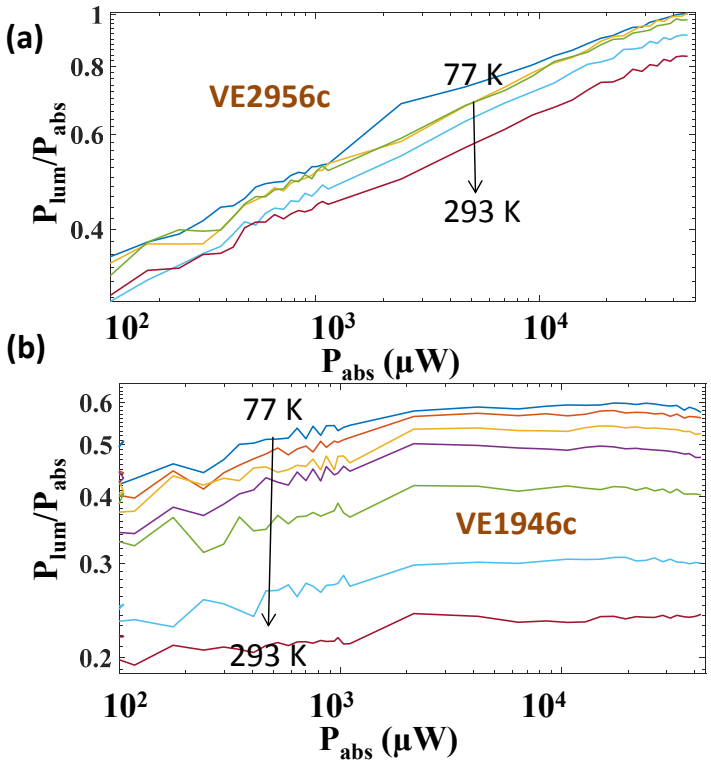

Figure 5 the internal quantum efficiency versus the 980 nm excitation power at various temperatures for (a) sample VE2956c and (b) sample VE1946c

Figure 6 while for sample VE1946c we could not obtain meaningful values due to the flatness of the curves. For this sample, comparing the time-resolved PL data with the intensity dependent quantum efficiency suggests that the radiative recombination is dominant and has a linear relationship with the carrier density in contrast to Eq (2). To the best of our knowledge two processes can be responsible for these phenomena, one of them is the excitonic superradiance and the other one is the impurity luminescence. To see whether the PL of VE1946 is due to the impurity luminesce we recorded the PL spectra at very low excitation power and we observed that the PL spectrum for both samples had a peak above the bandgap confirming that the PL is not coming from below-gap impurities. On the other hand considering the dopant luminescence efficiency of:

$$\eta_d = (\eta_e B N_d)/(A+\eta_e B N_d) \quad (9)$$

For the worst case scenario where N_d ,the dopant impurity concentration, is assumed it to be 10^{16} cm^{-3} with $A=10^5$ s^{-1} and $B=10^{-10}$ cm^3/s , we obtain the dopant luminescence efficiency to be around 23% which is still 2 times lower than what we obtained experimentally. Therefore we rule out the possibility of impurity and doping luminescence.

On the other hand, self-consistent Poisson-Schrodinger simulations confirm that the flatness of the quantum efficiency curve cannot be due to the screening of the built in electric field of the p-i-n structure of sample VE1946 nor due to change of quasi type-II band alignment for this range of the photogenerated carrier density. Therefore the only possibility is excitonic superradiance which justifies the exponential decay of the PL signal over time, the linear dependence of PL lifetime versus temperature as predicted by Eq(7) and also the flat curves of the internal

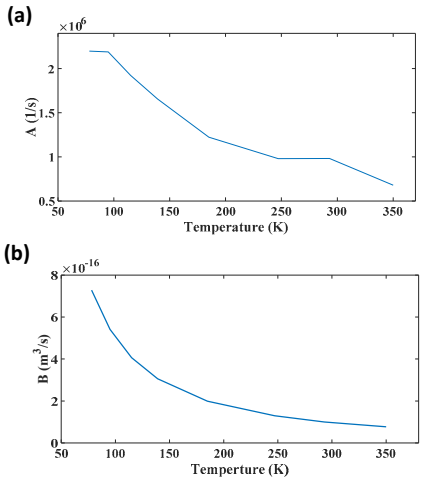

Figure 6 (a) The Shockley-Reed-Hall recombination coefficient (b) The radiative recombination rate of sample VE2956c

quantum efficiency (which is equal to $B_{ex}f_{ex}/(B_{ex}f_{ex}+A)$ where B_{ex} is excitonic radiative rate and f_{ex} is the fraction of the carriers which are excitons). The main question that remains is why we see this phenomenon in sample VE1946c and not the sample VE2956c? To answer this, we again take a look at the curves of Figure 5. These experiments indicate a significant increase of the internal quantum efficiency for sample VE2956c which can even get very close to 100% at low temperatures. We note that the introduced integrated setup does not provide a highly accurate estimation of the internal quantum efficiency because the exact extraction efficiency is not known and the integrated sphere is not ideal. Nonetheless it tells us that the quantum efficiency of sample VE2956c due to the free plasma is already high which can screen the excitonic effects. On the other hand for sample VE1946c we expect a much lower internal quantum efficiency since the overlap integral of the electron and hole wavefunction is lower as shown in the band diagram of Fig 7, and also it contains quaternary (InGaAsP) and InAlAs epitaxial layers with lower material quality and higher Schockly-Read-hall recombination rate. To estimate the fraction of excitons within the photogenerated carrier density, we used the Saha equation[12]:

$$K = \left(\frac{\mu}{2\pi\hbar^2}\right) K_B T exp\left(-\frac{E_b}{K_B T}\right) \tag{10a}$$

$$f_{ex} = 1 + \frac{K}{2n} - \sqrt{\frac{K}{2n}\left(\frac{K}{2n} + 2\right)} \tag{10b}$$

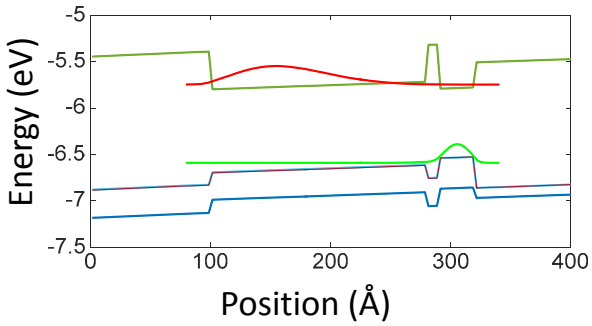

Figure 7 energy band diagram of sample VE1946c.

Where E_b is the exciton binding energy and n is the total photo-excited 2D carrier density. We found the binding energy for the QW structure based on Ref[13]. By performing this calculation we figured out that for sample VE1946c f_{ex} is 30% at 78 K and 9.6 % at room temperature. As a result, it is highly probable that this effect was detected in sample VE1946c since the excitonic super radiance decay rate is at least ten times higher than the plasma radiative rate.

4- Conclusions

In conclusion, we introduced the concept of excitonic super radiance for the purpose of optical refrigeration. To the best of our knowledge, the previous studies of excitonic effects have put the emphasis only on "Coulomb-induced steepening of absorption band-tail". This phenomenon can be employed to increase the optimum laser detuning and the cooling power and to overcome the adverse effects of parasitic absorption of the pump laser. Here, we showed that the excitonic radiative lifetime is much shorter than free carrier plasma in a quantum well structure. Although this looks very appealing however the thermal excess energy of the excitons which are able to radiate is quite low. Consequently we proposed the use of polaritonic crystals to be able to extract the energy of exciton polaritons with higher energy. A simple hexagonal photonic crystal structure was proposed and shown to increase the extraction efficiency significantly. The signature of excitonic super radiance decay was detected in one of our samples that showed exponential PL dynamics with lifetime that linearly increases with temperature. This sample also showed fairly intensity-independent internal quantum efficiency. Our next plan is to make a suitable polaritonic crystal on this sample and investigate its potential for the optical refrigeration of solids.

References

1 Mansoor Sheik-Bahae and Richard I Epstein, Nature Photonics **1** (12), 693 (2007).

2 Iman Hassani Nia and Hooman Mohseni, Applied Physics Letters **105** (4), 042102 (2014); I Hassani Nia, M Rezaei, R Brown, SJ Jang, A Turay, V Fathipour, and H Mohseni, Journal of Luminescence **170**, 841 (2016).

3 Richard I Epstein, Melvin I Buchwald, Bradley C Edwards, Timothy R Gosnell, and Carl E Mungan, Nature **377** (6549), 500 (1995).

4 Jun Zhang, Dehui Li, Renjie Chen, and Qihua Xiong, Nature **493** (7433), 504 (2013).

5 Mansoor Sheik-Bahae and Richard I Epstein, Physical review letters **92** (24), 247403 (2004).

6 Gunnar Björk, Stanley Pau, Joseph Jacobson, and Yoshihisa Yamamoto, Physical Review B **50** (23), 17336 (1994).

7 Lucio Claudio Andreani, Francesco Tassone, and Franco Bassani, Solid State Communications **77** (9), 641 (1991).

[8] Iman Hassani Nia and Hooman Mohseni, presented at the SPIE OPTO, 2014 (unpublished).
[9] Lucio Claudio Andreani, Physics Letters A **192** (1), 99 (1994).
[10] EL Ivchenko and AN Poddubnyĭ, Physics of the Solid State **48** (3), 581 (2006).
[11] SR Johnson, D Ding, J-B Wang, S-Q Yu, and Y-H Zhang, Journal of Vacuum Science & Technology B **25** (3), 1077 (2007).
[12] D Robart, X Marie, B Baylac, T Amand, M Brousseau, G Bacquet, G Debart, R Planel, and JM Gerard, Solid state communications **95** (5), 287 (1995).
[13] G Bastard, EE Mendez, LL Chang, and L Esaki, Physical Review B **26** (4), 1974 (1982).